Note

Second-sphere coordination of 5,5′-diamino-2,2′-bipyridine metal complexes with oxygen ligands through N–H···O hydrogen bonding

Xiao-Juan Yang [a], Biao Wu [a], Wen-Hua Sun [b], Christoph Janiak [a],*

[a] *Institut für Anorganische und Analytische Chemie, Universität Freiburg, Albertstr. 21, 79104 Freiburg, Germany*
[b] *State Key Laboratory of Engineering Plastics and Center for Molecular Sciences, Institute of Chemistry, Chinese Academy of Sciences, Beijing 100080, PR China*

Abstract

Tris(5,5′-diamino-2,2′-bipyridine)metal complexes, $[M(DABP)_3]^{2+}$ with M = nickel(II), zinc(II) or iron(II) can be engaged in hydrogen-bonding interactions from the amino groups to oxygen-containing molecules as H-bond acceptors. This so-called second-sphere coordination of the metal complexes is investigated here by using 18-crown-6 (18-C-6) and the 1,3,5-benzene-tricarboxylate (BTC) anion for N–H···O bonding. Single-crystal X-ray structural studies show that $[Ni(DABP)_3]^{2+}$ or $[Zn(DABP)_3]^{2+}$ and 18-C-6 form strands of alternating $[M(DABP)_3]^{2+}$ and 18-C-6 units with only two out of six amino groups getting involved in weak N–H···O bonding. The remaining NH_2 groups are hydrogen bonded to the chloride and nitrate anion, respectively, and solvent molecules of crystallization. The anionic BTC hydrogen-bond acceptor, however, is capable of capping the triangular face formed by the three amino groups in $[M(DABP)_3]^{2+}$. In $\{[Fe(DABP)_3]\cdot(BTC)_2\}^{4-}$ the capping occurs by two BTC units from both sides, i.e. for both triangular faces and engages all six NH_2 groups of the metal complex. Charge compensation is provided by two hydrated $\{[Fe(DABP)_3]\cdot aq\}^{2+}$ complexes per formula unit.
© 2002 Elsevier Science B.V. All rights reserved.

Keywords: Second-sphere coordination; Supramolecular chemistry; Hydrogen bonding; Crystal structures; Bipyridine complexes

1. Introduction

Second-sphere coordination, which refers to the non-covalent interaction, e.g. hydrogen bonding between metal complexes and external ligands, has attracted much interest because such host–guest interactions may lead to specific and effective modification of the spectral, electrochemical and other properties of the classical first-sphere metal complexes [1–6]. Crown ethers are the first and mostly studied macrocycles which serve as H-bond acceptors for the second-sphere coordination [7–12], while aqua- [13,14] or ammine- [7,9,15–21] metal complexes are often H-bond donors. There are a number of examples of second-sphere coordination in which a metal ammine complex

$(L_nM–NH_3)$ [15–20,22] or an alkylammonium ion $(R–NH_3^+)$ [8] was involved in the hydrogen-bonding; however, neutral organic amines $(R–NH_2, R_2–NH)$ as H-donors are very rare [23,24].

Herein, we report three second-sphere host–guest systems which are based on hydrogen-bonding from a neutral organic amine ligand $R–NH_2$. In the complexes the primary sphere ligand is 5,5′-diamino-2,2′-bipyridine (DABP) which chelates to the metal center by the pyridine nitrogen to form the metal complexes $[M(DABP)_3]^{2+}$ [23]. The neutral amino groups then bind to the second sphere ligand through multiple N–H···O hydrogen bonds. The H-bond acceptors, here, are 18-crown-6 (18-C-6) and 1,3,5-benzene-tricarboxylate (BTC), the trianion of trimesic acid (H_3BTC) which is frequently used in crystal engineering (Scheme 1) [25–30]. The complexes, thus, isolated are $\{[Ni(DABP)_3]\cdot(18-C-6)\}Cl_2\cdot4CH_3OH$ (**1**), $\{[Zn(DABP)_3]\cdot(18-C-6)\}(NO_3)_2\cdot3/8H_2O$ (**2**), and $[Fe(DABP)_3]_2\{[Fe(DABP)_3]\cdot(BTC)_2\}\cdot20H_2O$ (**3**).

* Corresponding author. Tel.: +49-761-203 6127; fax: +49-761-203 6147

E-mail address: janiak@uni-freiburg.de (C. Janiak).
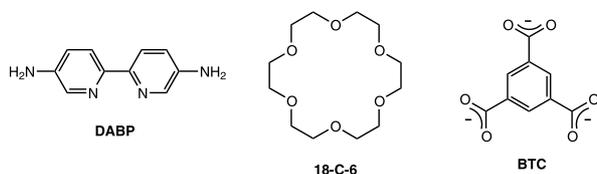
Scheme 1. Hydrogen-bond donor (5,5′-diamino-2,2′-bipyridine, DABP) and acceptor moieties (18-C-6 and BTC) used in this work.

Our goal is to cap each triangular face formed by the three amino groups in $[M(DABP)_3]^{2+}$ with an (18-C-6) or BTC cover, as shown in Scheme 2. The second-sphere hydrogen bonding from the amino groups to the oxygen atoms of 18-C-6 or BTC should create a molecular container.

2. Experimental

NMR spectra were recorded on a Bruker Avance DPX200 or a Varian Unity-300 spectrometer (200.1 or 300.1 MHz, respectively) with calibration against the solvent signal (DMSO-d_6 2.50 ppm). The numbering for the NMR notation of the bipyridine ligands for **2** and **3** is as in Scheme 3. Elemental analysis were done on a VarioEL from Elementaranalysensysteme GmbH. Electron spray ionization mass spectra (ESI-MS) were carried out using a Finnigan MAT LCQ Advantage. Acetonitrile, MeCN was used as a solvent. Mass spectra were measured in positive mode and in the range of $m/z = 100$–2000. Metal containing ions had a clearly visible metal isotope pattern arising from the distribution: ^{54}Fe 6.3, ^{56}Fe 100, ^{57}Fe 2.4%; ^{58}Ni 100, ^{60}Ni 38.2, ^{62}Ni 5.3%.

The ligand 5,5′-diamino-2,2′-bipyridine and its metal complexes, $[Fe(DABP)_3]SO_4$, $[Ni(DABP)_3]Cl_2$, and $[Zn(DABP)_3](NO_3)_2$ were prepared following previously
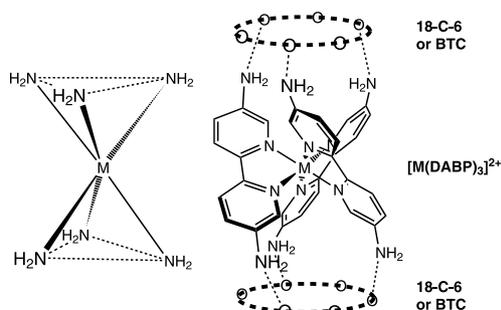
Scheme 2. Planned second-sphere supramolecular assembly of $[M(DAPB)_3]^{2+}$ with 18-C-6 or BTC.
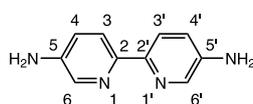
Scheme 3. Numbering scheme for bipyridines.

published procedures [23,31]. 18-C-6 and H_3BTC were purchased from Acros and used as received.

2.1. Preparation of $\{[Ni(DABP)_3]\cdot(18\text{-}C\text{-}6)\}Cl_2\cdot 4CH_3OH$ (**1**)

A solution of $[Ni(DABP)_3]Cl_2$ (34 mg, 0.05 mmol) in 3 ml of MeOH was combined with 1 ml of a methanolic solution of 18-C-6 (13 mg, 0.05 mmol). To the mixture was added 3 ml of isopropanol, which resulted in a clear pale red solution. The solvent was then allowed to slowly evaporate at room temperature (r.t.). After several days, well-shaped red prismatic crystals formed which were suitable for X-ray single crystal analysis. Crystal yield: 33 mg, 70%. ESI-MS: m/z (Intensity%, fragment) 308 (100, $[Ni(DABP)_3]^{2+}$), 235 (37, $[Ni(DABP)_2(MeCN)]^{2+}$). *Anal.* Found: C, 52.75; H, 5.50; N, 17.82. Calc. for $C_{42}H_{54}Cl_2N_{12}NiO_6$: C, 52.96; H, 5.71; N, 17.65%.

2.2. Preparation of $\{[Zn(DABP)_3]\cdot(18\text{-}C\text{-}6)\}(NO_3)_2\cdot 3/8H_2O$ (**2**)

The zinc complex was prepared by a similar procedure except that $[Zn(DABP)_3](NO_3)_2$ (37 mg, 0.05 mmol) was used instead of $Ni(DABP)_3Cl_2$. Yellow cubic crystals of compound **2** were obtained. Crystal yield 27 mg, 54%. ^{1}H NMR: (DMSO-d_6, δ ppm): 8.11 (d, 6H, $J = 8.8$ Hz, H3,3′), 7.28 (dd, 6H, $J_1 = 8.8$ Hz, $J_2 = 2.4$ Hz, H4,4′), 7.16 (d, 6H, $J = 2.4$ Hz, H6,6′), 6.02 (s, 12H, –NH$_2$), 3.58 (s, 24H, O–CH$_2$–CH$_2$–O). *Anal.* Found: C, 49.60; H, 5.36; N, 19.17. Calc. for $C_{42}H_{54}N_{14}O_{12}Zn$: C, 49.83; H, 5.38; N, 19.37%.

2.3. Preparation of $[Fe(DABP)_3]_2\{[Fe(DABP)_3]\cdot(BTC)_2\}\cdot 20H_2O$ (**3**)

$[Fe(DABP)_3]SO_4$ (36 mg, 0.05 mmol) was reacted with $Ba(OH)_2\cdot 8H_2O$ (16 mg, 0.05 mmol) by stirring the two materials in 5 ml of water for 0.5 h. The precipitated $BaSO_4$ was removed by filtration. To the filtrate solution of the in situ prepared $[Fe(DABP)_3](OH)_2$ was added trimesic acid H_3BTC (7 mg, 0.033 mmol). The slurry was stirred overnight at r.t. to form a red precipitate. The precipitate was collected, washed with H_2O, and recrystallized from hot H_2O to form red hexagonal platelets of compound **3**. Crystal yield: 23 mg, 61%. ^{1}H NMR (DMSO-d_6, δ ppm): 8.36 (s, 6H, 2 equiv. of $C_6H_3(COO)_3^{3-}$), 7.99 (d, 18 H, $J = 8.8$ Hz, H3,3′), 7.06 (dd, 18H, $J_1 = 8.8$ Hz, $J_2 = 2.2$ Hz, H4,4′), 6.58 (d, 18H, $J = 2.2$ Hz, H6,6′), 5.91 (s, 36H, –NH$_2$). ESI-MS: m/z (Intensity%, fragment) 307 (100, $[Fe(DABP)_3]^{2+}$), 234 (56, $[Fe(DABP)_2(MeCN)]^{2+}$). *Anal.* Found: C, 51.87; H, 4.75; N, 19.32. Calc. for $[Fe(DABP)_3]_3\cdot(BTC)_2\cdot 15H_2O$ ($C_{108}H_{126}Fe_3N_{36}O_{27}$): C, 51.31; H, 5.02; N, 19.95%.

2.4. Crystal data collection and structure determination

Diffraction data were collected by the ω-scan method with Mo Kα radiation ($\lambda = 0.71073$ Å) and the use of a graphite monochromator on a Siemens Bruker Smart AXS CCD for complexes **1** and **3** and a Bruker Smart 1000 diffractometer for compound **2**. The structures were solved by direct methods (SHELXS-97) [32]. For **1** and **3** refinement was done by full-matrix least-squares, for **2** by block-matrix least-squares on F^2 using the SHELXL-97 program suite [32]. All non-hydrogen positions were found and refined with anisotropic temperature factors. Hydrogen atoms were calculated using appropriate riding models [AFIX 93 for NH$_2$, d(N–H) = 0.87, AFIX 43 for aromatic CH, AFIX 23 for CH$_2$] and isotropic temperature factors of U(H) = 1.2 U_{eq}(C). In **1** the hydrogen atoms on the crown ether carbon atoms C20, C21 and on the crystal solvent methanol molecules could not be calculated. In **1** the oxygen atom O3 of the crown ether is disordered, the other position being O3′ (not shown in Fig. 1 for clarity). In 18-C-6, the C–C and O–C bond distances, respectively, are restrained to be equal. In **2** the hydrogen atoms of the crystal water molecules were not included and the thermal displacement parameters of the crown ether and nitrate atoms were kept fixed in the final cycles. In **3** the hydrogen atoms of the crystal water molecules could not be calculated.

A notable feature of the structures reported here is that they crystallize in the chiral space groups $C222_1$ (**1**), $P2_1$ (**2**), and $R3c$ (**3**). The structures were refined as twins. In **1** refinement was successful as an orthorhombic twin with a and b approximately equal in length to emulate tetragonal (twin law 0 1 0, 1 0 0, 0 0 −1). The batch scale factor (BASF) for unequal components in a

Fig. 1. Hydrogen bonding interactions between [Ni(DABP)$_3$]$^{2+}$ and 18-C-6 in **1**; see Table 2 for details. Additional H-bonds from the amino groups to the chloride anion and the MeOH solvent molecules in **1** are not shown. The kinked chains run along c. Carbon atoms are depicted as small spheres for better visibility of the H-bonds. The disordered position to O3 (O3′) is not shown for clarity. Symmetry relation a = −x+1, −y, z+1/2; a′ = −x+1, −y, z−1/2. For b, c, d; see footnote to Table 2.

twin refinement was 0.26(3). For **2** the TWIN instruction with the default matrix (−1 0 0, 0 −1 0, 0 0 −1) was used and BASF refined to 0.38(2) for the selected crystal. For **3** the crystal structure was refined as a racemic twin [BASF = 0.48(6)]. Crystal data are listed in Table 1. Graphics were obtained with ORTEP 3 for Windows [33]. Displacement ellipsoids are drawn at the 50% probability level and H atoms are shown as spheres of arbitrary radii. Special computations for the crystal structure discussions were carried out with PLATON for Windows [34].

3. Results and discussion

In compound **1**–**3** the metal center is hexa-coordinated by the nitrogen atoms of the three bipyridine chelate ligands. Such a tris(chelate) structure is unremarkable for [M(bipy)$_3$]$^{2+}$ complexes (bipy = 2,2′-bipyridine) and a sizable number of examples are available (Fe, [35–38]; Ni, [38–41]; Zn, [42–45]). Specifically the metal environment in [M(DABP)$_3$]$^{2+}$ has been discussed recently in the parent compounds [Fe(DABP)$_3$]SO$_4$, [Ni(DABP)$_3$]Cl$_2$ and [Zn(DABP)$_3$]-(NO$_3$)$_2$ [23] and in other complexes with 5,5′-disubstituted bipyridine ligands [46,47].

Here, we are interested in the second-sphere coordination of the cationic [M(DABP)$_3$]$^{2+}$ complexes. The amino groups of the DABP–ligand have already been found to enter in N–H$\cdots$O hydrogen bonding to water molecules of crystallization or in N–H$\cdots$X hydrogen bonding to anions (X = SCN$^-$, SO$_4^{2-}$, Cl$^-$) or acceptor ligands in M(DABP)$_y$X$_2$ moieties (X = Cl, N$_3$) [23]. In the present study, 18-C-6 or BTC were offered as acceptor molecules for (N–H$\cdots$O) hydrogen bonding from the amino groups.

In the crystal structure of compound **1** (shown in Fig. 1), two out of the six amino groups of the [Ni(DABP)$_3$]$^{2+}$ moiety form multiple hydrogen bonds with the oxygen atoms of a crown ether. The two amino groups (N4 and N4^c) are located on two different, albeit symmetry related bipyridine ligands. Each of these two amino groups binds to one 18-C-6 molecule. The H-bonding in **1** is rather weak with the N(–H)$\cdots$O contacts being largely well above 3.0 Å (see Table 2). For each 18-C-6 a second amino group from another, symmetry related [Ni(DABP)$_3$]$^{2+}$ unit binds to the ethereal oxygen atoms from the opposite side of the crown ether molecule. Thus, the first-sphere complex [Ni(DABP)$_3$]$^{2+}$ and the second-sphere ligand 18-C-6 form a kinked, 2_1-helical chain structure. Each strand contains only chiral [Ni(DABP)$_3$]$^{2+}$ molecules of the same handedness [48] (Λ in Fig. 1). The remaining four amino groups of a [Ni(DABP)$_3$]$^{2+}$ unit, which are not involved in hydrogen bonding with the crown ether, interact through hydrogen bonding with the chloride

Table 1
Crystal data and structure refinement for compounds **1**, **2**, and **3**

Compound	{[Ni(DABP)$_3$] (18-C-6)}Cl$_2$·4CH$_3$OH (**1**)	{[Zn(DABP)$_3$]·(18-C-6)}(NO$_3$)$_2$·3/8H$_2$O (**2**)	{[Fe(DABP)$_3$]$_3$·(BTC)$_2$} 20H$_2$O (**3**)
Empirical formula	C$_{46}$H$_{70}$Cl$_2$N$_{12}$NiO$_{10}$	C$_{168}$H$_{219}$N$_{56}$O$_{49.5}$Zn$_4$	C$_{108}$H$_{136}$Fe$_3$N$_{36}$O$_{32}$
M (g mol^{-1})	1080.75	4076.45	2618.03
Crystal description	prismatic	cubic	platelet
Crystal color	red	yellow	red
Temperature (K)	210(2)	293(2)	208(2)
Crystal system	orthorhombic	monoclinic	rhombohedral
Space group	$C222_1$	$P2_1$	$R3$c
Unit cell dimensions			
a (Å)	17.9002(14)	19.975(3)	28.6167(14)
b (Å)	17.9370(14)	21.699(3)	28.6167(14)
c (Å)	16.9267(14)	24.770(4)	28.6167(14)
α (°)	90	90	32.745(1)
β (°)	90	104.585(4)	32.745(1)
γ (°)	90	90	32.745(1)
V (Å^3)	5434.8(8)	10 390(3)	6099.1(5)
Z	4	2	2
D_{calc} (g cm^{-3})	1.321	1.301	1.426
$F(000)$	2288	4258	2740
Crystal size (mm)	0.20 × 0.20 × 0.15	0.30 × 0.25 × 0.20	0.40 × 0.40 × 0.02
2θ Range (°)	2.4–50.1	1.7–50.1	3.1–56.7
Index range	$-13 \le h \le 21$; $-21 \le k \le 20$; $-20 \le l \le 17$	$-23 \le h \le 23$; $-20 \le k \le 25$; $-29 \le l \le 26$	$-38 \le h \le 28$; $-38 \le k \le 30$; $-38 \le l \le 23$
Absorption coefficient (mm^{-1})	0.520	0.543	0.444
Absorption correction	SADABS [49]	semi-empirical from equivalents	SADABS [49]
Max/min transmission	0.9261/0.9032	0.8992/0.8540	0.9912/0.8424
Reflections collected	14 092	43 707	36 575
Independent reflections	4831 [$R_{int} = 0.0377$]	27 433 [$R_{int} = 0.0753$]	7865 [$R_{int} = 0.0712$]
Observed reflections [$I > 2\sigma(I)$]	4158	11 755	4146
Completeness to theta	25.06°, 100.0%	25.03°, 99.9%	28.34°, 98.6%
Parameters refined	332	2441	534
Max./min. Δρ ^{a} (e Å^{-3})	0.618/−0.372	1.020/−1.583	0.953/−0.549
R_1/wR_2 ^{b} [$I > 2\sigma(I)$]	0.0423/0.0991	0.1141/0.2926	0.0823/0.2959
R_1/wR_2 ^{b} (all reflections)	0.0541/0.1062	0.2302/0.3685	0.1511/0.2534
Goodness-of-fit on F^2 ^{c}	1.037	1.040	1.068
Flack parameter [50] ^{d}	0.26(3)	0.38(2)	0.48(6)
Weighting scheme w; a/b ^{e}	0.0566/0.0000	0.2000/0.0000	0.1686/0.3225

^{a} Largest difference peak and hole.
^{b} $R_1 = [\Sigma \, (||F_o| - |F_c||)/\Sigma \, |F_o|]$; $wR_2 = [\Sigma \, [w(F_o^2 - F_c^2)^2]/\Sigma \, [w(F_o^2)^2]]^{1/2}$.
^{c} Goodness-of-fit $= [\Sigma \, [w(F_o^2 - F_c^2)^2]/(n-p)]^{1/2}$.
^{d} Batch scale factor (BASF) for unequal components in twin refinement; BASF = 0.5 corresponds to racemic twinning.
^{e} $w = 1/[\sigma^2(F_o^2) + (aP)^2 + bP]$ where $P = (\max(F_o^2 \text{ or } 0) + 2F_c^2)/3$.

anion or the methanol solvent molecules. Details of the H-bonding scheme for **1** are given in Table 2.

Compound **2** also shows a 1:1 stoichiometric ratio of the metal complex [Zn(DABP)$_3$]$^{2+}$ and 18-C-6, but its second-sphere structure is different from that of the Ni analogue. There are four independent [Zn(DABP)$_3$]$^{2+}$ units and four crown ethers in a unit cell. Similar to compound **1**, two amino groups in each [Zn(DABP)$_3$]$^{2+}$ unit form hydrogen bonds with two crown ethers, however, these two H-bond donors are from the same bipyridine ligand. Each amino group binds to 2–4 mostly adjacent oxygen atoms (with N···O < 3.3 Å) of a crown ether (Fig. 2, Table 3). The opposite face of the crown ether with the remaining oxygen atoms is then coordinated by an amino group from another, independent [Zn(DABP)$_3$]$^{2+}$ complex. Short N···O contacts to one face correlate with long N···O contacts to the other face of the crown ether. This results in a linear chain arrangement with tilted crown ether molecules (Fig. 2 and Scheme 4). It can be noted that each strand contains only chiral [Zn(DABP)$_3$]$^{2+}$ molecules of the same handedness. The strand shown in Fig. 2 contains [Zn(DABP)$_3$]$^{2+}$ molecules in the Λ-configuration. The strand composed of the other two independent [Zn(DABP)$_3$]$^{2+}$ and crown ether units (Scheme 4) contains the complex cations in the Δ-configuration

Table 2
Selected hydrogen bonding interactions from the NH$_2$ groups in **1**[i]

D–H···A	d(D···A) (Å)
N4–H4A···O1	3.24(1)
N4–H4A···O2	3.40(1)
N4–H4B···O2[b]	3.05(1)
N4–H4B···O3[b ii]	3.69(1)
N4–H4B···O3'[,b ii]	3.16(1)
N6–H6A···O4[c] (MeOH)	3.08(1)
N2–H2B···O5[c] (MeOH)	2.99(1)
N2–H2A···Cl1[d]	3.29(1)
N6–H6B···Cl2	3.27(1)

[i]Only D···A distances are given since the H atom positions were calculated. Symmetry relations b = −x+1, y, −z+3/2; c = x, −y, −z+1; d = −x+3/2, −y+1/2, z−1/2. [ii]The hydrogen bond to N4–H4B···O3[b] and the disordered position O3' is not shown in Fig. 1.
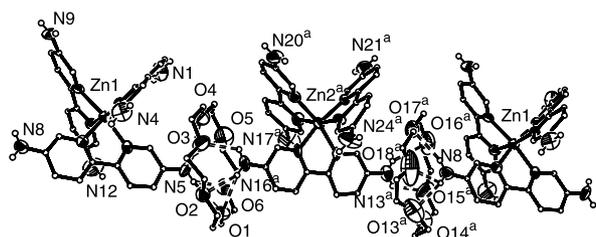
Fig. 2. Hydrogen bonding interactions between [Zn(DABP)$_3$]$^{2+}$ and 18-C-6 in **2**; see Table 3 for details. Only one of the two independent strands is shown. Additional H-bonds from the amino groups to the nitrate anion and the water molecules in **2** are not shown. The chains run along *c*. Carbon atoms are depicted as small spheres for better visibility of the H-bonds. Symmetry relation a = 1−x, y−1/2, 1−z; a' = x, y, z+1.

[48]. Details of the H-bonding scheme for **2** are given in Table 3. It should be noted that the amino groups are bound largely to three adjacent oxygen atoms in the crown ether instead of every second oxygen atom as can be found in other crown ether adducts, e.g. [PtCl$_2$(PMe$_3$)(NH$_3$)]$_2$·(18-C-6) [7].

In variance to our goal depicted in Scheme 2, only one amine in each triangular face of [M(DABP)$_3$]$^{2+}$ becomes involved in hydrogen bonding to the crown ether. Such incomplete intermolecular binding of the first sphere complexes has been found in several crown ether adducts [7–9]. Moreover, the H-bond interactions between the amino group and the crown ether are quite weak with N(–H)···O contacts mostly longer than 3.0 Å. In order to arrive at the desired bonding model from Scheme 2 and strengthen the H-bonds, we chose the BTC trianion as the H-bond acceptor.

Cocrystallization of 3 equiv. of [Fe(DABP)$_3$](OH)$_2$ with 2 equiv. of trimesic acid (H$_3$BTC) yielded well-formed red hexagonal plates. The space group symmetry (*R*3c) reflects the trigonal symmetry of the molecular building blocks. The crystal structure is built from [Fe(DABP)$_3$]$^{2+}$ and BTC^{3-} in a ratio of 3:2 so that no further anions are required. One-third of the

Table 3
Selected hydrogen bonding interactions from the NH$_2$ groups in **2**[i]

D–H···A	d(D···A) (Å)
N5–H5A···O6	2.99(2)
N5–H5A···O1	3.35(2)
N5–H5B···O5	3.26(2)
N5–H5B···O4	3.19(2)
N8'–H8A···O17[a]	3.26(2)
N8'–H8B···O18[a]	2.95(2)
N8'–H8B···O13[a]	3.33(2)
N4–H4B···O28[b] (NO$_3$)	2.95(2)
N12–H12A···O50 (H$_2$O)	3.25(2)
N13–H13A···O16	3.21(2)
N13–H13B···O15	3.05(2)
N16[a]–H16A···O2	3.25(2)
N16[a]–H16A···O1	3.21(2)
N16[a]–H16B···O3	3.10(2)
N17–H17A···O11	3.29(2)
N17–H17B···O43 (NO$_3$)	2.96(2)
N20–H20A···O27[c] (NO$_3$)	2.86(2)
N20–H20B···O49[d] (H$_2$O)	2.88(2)
N21–H21A···O44 (NO$_3$)	2.85(2)
N21–H21B···O29[a] (NO$_3$)	3.06(2)
N21–H21B···O30[a] (NO$_3$)	3.33(2)
N24–H24A···O41[c] (NO$_3$)	3.06(2)

[i]Only D···A distances are given since the H atom positions were calculated. Symmetry relations a = −x+1, y+1/2, −z+1; ' = x, y, z+1; b = −x, y−1/2, −z+1; c = x+1, y, z; d = −x+2, y+1/2, −z+1.
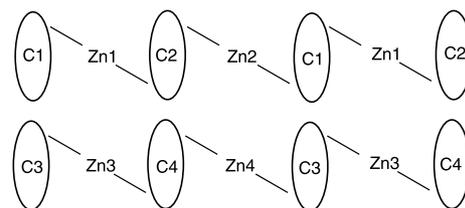
Scheme 4. Schematic packing between [Zn(DABP)$_3$]$^{2+}$ and 18-C-6 in **2**.

[Fe(DABP)$_3$]$^{2+}$ units are fully involved in the hydrogen bonding with BTC^{3-}. There the metal complex cation has its two triangular faces, each formed by three amino groups, capped by two BTC anions (see Scheme 2). Each amine is hydrogen-bonded to an oxygen atom of a carboxylate group. Thus, the [Fe(DABP)$_3$]$^{2+}$ moiety is encapsulated by two molecules of the tricarboxylate anion (Fig. 3). This *C*$_3$-symmetrical {[Fe(DABP)$_3$]·(BTC)$_2$}$^{4-}$ arrangement represents a chiral entity. The complex molecules shown in Fig. 3 exhibit the Δ-configuration.

For each carboxylate group, only one oxygen forms a hydrogen bond with the amino group and the other O atom is involved in hydrogen bonding with the water of crystallization. In order to balance the charge, the other two-thirds of the [Fe(DABP)$_3$]$^{2+}$ units are not complexed by the second-sphere ligand BTC. Instead, they
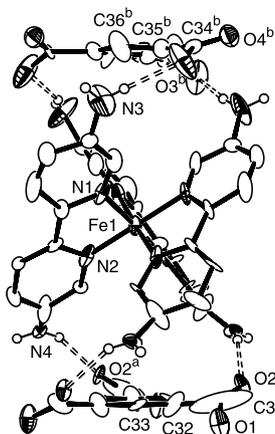
Fig. 3. Hydrogen bonding interactions between $[Fe(DABP)_3]^{2+}$ and BTC in the anionic $\{[Fe(DABP)_3]\cdot(BTC)_2\}^{4-}$ moiety of **3**; see Table 4 for details.

Table 4
Selected hydrogen bonding interactions from the NH_2 groups in **3**[i]

D–H···A	d(D···A) (Å)
N3–H3A···O3[b]	2.90(2)
N3–H3B···O01[c] (H_2O)	2.88(2)
N4–H4A···O2[a]	2.95(2)
N4–H4B···O02[d] (H_2O)	3.05(2)
N7–H7B···O01 (H_2O)	2.87(2)
N8–H8A···O2[e]	3.25(2)
N8–H8B···O08[f] (H_2O)	3.02(2)
N11–H11A···O07 (H_2O)	2.91(2)
N11–H11B···O3[g]	3.00(2)
N12–H12A···O08 (H_2O)	3.36(2)
N12–H12B···O02 (H_2O)	3.00(2)

[i] Only D···A distances are given since the H atom positions were calculated. Symmetry relations a $= y$, z, $x+1$; b $= y+1/2$, $x-1/2$, $z+1/2$; c $= x+1/2$, $z+1/2$, $y-1/2$; d $= x-1/2$, $z+1/2$, $y-1/2$; e $= x+1/2$, $z-1/2$, $y+1/2$; f $= z$, $x-1$, y; g $= z+1$, x, y.

form hydrogen bonds to water molecules through the amino groups. In the crystal structure the capped anionic $\{[Fe(DABP)_3](BTC)_2\}^{4-}$ complexes are, thus, surrounded by hydrated $[Fe(DABP)_3]^{2+}$ cations with two different iron centers. Fig. 4 illustrates a section of the packing diagram. There is hydrogen bonding also between the crystal water and the free oxygens of the BTC anion and the free N–H's of the $\{[Fe(DABP)_3]\cdot(BTC)_2\}^{4-}$ moiety. Hydrogen bonding among the water of crystallization which also involves free water molecules completes the supramolecular packing arrange-

ment. Selected hydrogen bonding interactions are listed in Table 4.

A second-sphere coordination similar to **3** was reported in which the first sphere complexes are hexaaqua metal ions $[M(H_2O)_6]^{3+}$ and the second-sphere ligand is the trianion of 1,3,5-tris(sulfo-methyl)benzene (L) [14]. In the structure of formula $[Fe(H_2O)_6]\{[Fe(H_2O)_6]\cdot(L)_2\}\cdot6MeOH$ half of the $[Fe(H_2O)_6]^{3+}$ centers were encapsulated by the ligand L and the other half of the Fe^{3+} centers provided a charge compensation. In the present work the divalent complex $[Fe(DABP)_3]^{2+}$ was used to bind the trianion BTC^{3-} and therefore one-third of the $Fe(DABP)_3^{2+}$ units form the encapsulated structure. It is obvious that the first-sphere complexes $[M(DABP)_3]^{2+}$ have a favorable pre-organized conformation of the triangular faces formed by three amines, which can recognize appropriate tripodal second-sphere ligands to form supramolecular complexes. Further investigation of the second-sphere complexes, e.g. the solution behavior and the effect of the non-covalent interaction on the properties of the complexes is in progress.

Fig. 4. Section of the packing diagram between the three different $[Fe(DABP)_3]^{2+}$ cations, the two different BTC^{3-} anions and the crystal water molecules in **3**. Dashed lines indicate hydrogen bonding interactions between $[Fe(DABP)_3]^{2+}$ and BTC^{3-}. Other hydrogen bonding interactions are not shown for clarity. Each capped $\{[Fe(DABP)_3]\cdot(BTC)_2\}^{4-}$ moiety (Fe1) is 'octahedrally' surrounded by hydrated $[Fe(DABP)_3]^{2+}$ cations ($3 \times$ Fe2, $3 \times$ Fe3). The schematic drawing to the right should illustrate the ABC type packing arrangement in the 110-plane which gives rise to the skewed rhombohedral unit cell with $\alpha = \beta = \gamma = 32.745°$.

4. Supplementary material

Crystallographic data for the structural analysis have been deposited with the Cambridge Crystallographic Data Centre, CCDC Nos. 185555–185557 for compounds **1**, **2** and **3**, respectively. Copies of this information may be obtained free of charge from The Director, CCDC, 12 Union Road, Cambridge, CB2 1EZ, UK (fax: +44-1223-336-033; e-mail: deposit@ccdc.cam.ac.uk or www: http://www.ccdc.cam.ac.uk).

References

[1] S.J. Loeb, in: J.L. Atwood, J.E.D. Davies, D.D. MacNicol, F. Vögtle (Eds.), Comprehensive Supramolecular Chemistry, vol. 1, Elsevier Science, New York, 1996, p. 733.

[2] F.M. Raymo, J.F. Stoddart, Chem. Ber. 129 (1996) 981.

[3] H.M. Colquhoun, J.F. Stoddart, D.J. Williams, Angew. Chem., Int. Ed. Engl. 25 (1986) 487.

[4] M. Botta, Eur. J. Inorg. Chem. (2000) 399.

[5] K. Zamaraev, New. J. Chem. 18 (1994) 3.

[6] J.W. Steed, Coord. Chem. Rev. 215 (2001) 171.

[7] H.M. Colquhoun, D.F. Lewis, J.F. Stoddart, D.J. Williams, J. Chem. Soc., Dalton Trans. (1983) 607.

[8] A.L. Crumbliss, I. Batinic-Haberle, I. Spasojevic, Pure Appl. Chem. 68 (1996) 1225.

[9] X.L. Zhang, D.I. Yoon, J.T. Hupp, Inorg. Chim. Acta 240 (1995) 285.

[10] S. Kannan, S.S. Raj, H.K. Funk, Polyhedron 20 (2001) 2145.

[11] P.C. Junk, J.L. Atwood, J. Organomet. Chem. 565 (1998) 179.

[12] I. Batinic-Haberle, I. Spasojevic, A.L. Crumbliss, Inorg. Chim. Acta 260 (1997) 35.

[13] U. Auerbach, C. Stockheim, T. Weyhermüller, K. Wieghardt, B. Nuber, Angew. Chem., Int. Ed. Engl. 32 (1993) 714.

[14] S.A. Dalrymple, M. Parvez, G.K.H. Shimizu, Chem. Commun. (2001) 2672.

[15] H.M. Colquhoun, J.F. Stoddart, D.J. Williams, Angew. Chem., Int. Ed. Engl. 20 (1981) 1051.

[16] B.R. Cameron, S.S. Corrent, S.J. Loeb, Angew. Chem., Int. Ed. Engl. 34 (1995) 2689.

[17] J.E. Kickham, S.J. Loeb, Inorg. Chem. 36 (1995) 5656.

[18] D.R. Alston, T.H. Lilley, J.F. Stoddart, J. Chem. Soc., Chem. Commun. (1985) 1600.

[19] D.R. Alston, A.M.Z. Slawin, J.F. Stoddart, D.J. Williams, J. Chem. Soc., Chem. Commun. (1985) 1602.

[20] I. Ando, M. Higashi, K. Ujimoto, H. Kurihara, Inorg. Chim. Acta 282 (1999) 247.

[21] I. Ando, K. Ujimoto, H. Kurihara, Bull. Chem. Soc. Jpn. 74 (2001) 717.

[22] H. Kurosawa, H. Asano, Y. Miyaki, Inorg. Chim. Acta 270 (1998) 87.

[23] C. Janiak, S. Deblon, H.-P. Wu, M.J. Kolm, P. Klüfers, H. Piotrowski, P. Mayer, Eur. J. Inorg. Chem. (1999) 1507.

[24] J.E. Kickham, S.J. Loeb, S.L. Murphy, Chem. Eur. J. 3 (1997) 1203.

[25] S.V. Kolotuchin, P.A. Thiessen, E.E. Fenlon, S.R. Wilson, C.J. Loweth, S.C. Zimmerman, Chem. Eur. J. 5 (1999) 2537.

[26] D.J. Plaut, K.M. Lund, M.D. Ward, Chem. Commun. (2000) 769.

[27] S.S.-Y. Chui, S.M.-F. Lo, J.P.H. Charmant, A.G. Orpen, I.D. Williams, Science 283 (1999) 1148.

[28] D. Braga, A. Angeloni, E. Tagliavini, F. Grepioni, J. Chem. Soc., Dalton Trans. (1998) 1961.

[29] O.M. Yaghi, C.E. Davis, G. Li, H. Li, J. Am. Chem. Soc. 119 (1997) 2861.

[30] C. Daiguebonne, O. Guilloa, Y. Gérault, A. Lecerf, K. Boubekeur, Inorg. Chim. Acta 284 (1994) 139.

[31] C. Janiak, S. Deblon, H.-P. Wu, Synth. Commun. 29 (1999) 3341.

[32] G.M. Sheldrick, SHELXS-97, SHELXL-97, Programs for Crystal Structure Analysis, University of Göttingen, Göttingen, Germany, 1997.

[33] (a) M.N. Burnett, C.K. Johnson, ORTEP-III: Oak Ridge Thermal Ellipsoid Plot Program for Crystal Structure Illustrations, Oak Ridge National Laboratory Report ORNL-6895, Oak Ridge, TN, 1996;
(b) L.J. Farrugia, ORTEP 3 for Windows, Version 1.0.1β, University of Glasgow, Glasgow, 1997;
(c) L.J. Farrugia, J. Appl. Crystallogr. 30 (1997) 565.

[34] (a) A.L. Spek, Acta Crystallogr., A 46 (1990) C34;
(b) L.J. Farrugia, PLATON Version 29-11-98, Windows implementation: University of Glasgow, Glasgow, 1998.

[35] H.L.K. Wah, M. Postel, F. Tomi, L. Mordenti, D. Ballivet-Tkatchenko, F. Dahan, F. Urso, New J. Chem. 15 (1991) 629.

[36] S. Bernès, F. Sécheresse, Y. Jeannin, Inorg. Chim. Acta 194 (1992) 105.

[37] H.W. Schmalle, R. Pellaux, S. Decurtins, Z. Kristallogr. 211 (1996) 533.

[38] S. Decurtins, H.W. Schmalle, P. Schneuwly, J. Ensling, P. Gütlich, J. Am. Chem. Soc. 116 (1994) 9521.

[39] P. Román, C. Guzmán-Miralles, A. Luque, J. Chem. Soc., Dalton Trans. (1996) 3985.

[40] J. Cernak, E. Lenyelova, K. Ahmadi, A.-M. Hardy, J. Coord. Chem. 37 (1996) 55.

[41] J. Cernak, M. Kanuchova, J. Chomic, I. Potocnak, J. Kamenicek, Z. Zak, Acta Crystallgr., C 50 (1994) 1563.

[42] S. Baggio, M.I. Pardo, R. Baggio, M.T. Garland, Acta Crystallgr., C 53 (1997) 1570.

[43] U. Klement, D. Trumbach, H. Yersin, Z. Kristallogr. 210 (1995) 228.

[44] X.-M. Chen, R.-Q. Wang, X.-L. Yu, Acta Crystallogr., C 51 (1995) 1545.

[45] E. Krausz, H. Riesen, A.D. Rae, Aust. J. Chem. 48 (1995) 929.

[46] H.-P. Wu, C. Janiak, G. Rheinwald, H. Lang, J. Chem. Soc., Dalton Trans. (1999) 183.

[47] X.-J. Yang, C. Janiak, J. Heinze, F. Drepper, P. Mayer, H. Piotrowski, P. Klüfers, Inorg. Chim. Acta 318 (2001) 103.

[48] C. Janiak, in Moderne Anorganische Chemie E. Riedel (ed.), W de Gruyter, Berlin, 1999, pp. 185–186.

[49] G. Sheldrick, Program SADABS: Area-detector absorption correction, University of Göttingen, Göttingen, Germany, 1996.

[50] H.D. Flack, Acta Crystallgr., A 39 (1983) 876.